Available online at www.sciencedirect.com

ScienceDirect

Advances in Space Research 73 (2024) 5017–5030

ADVANCES IN SPACE RESEARCH (a COSPAR publication)

www.elsevier.com/locate/asr

Refined troposphere delay models by NWM ray-tracing for pseudolite positioning system and their performance assessment

Wenjie Tang [a,b], Junping Chen [a,b,*], Yize Zhang [a], Junsheng Ding [a,b], Ziyuan Song [a,b]

[a] Shanghai Astronomical Observatory, Chinese Academy of Sciences, Shanghai 200030, China
[b] School of Astronomy and Space Science, University of Chinese Academy of Sciences, Beijing 100049, China

Received 23 November 2023; received in revised form 23 January 2024; accepted 19 February 2024
Available online 21 February 2024

Abstract

Pseudolite positioning system can enhance GNSS (Global Navigation Satellite System) by improving satellite geometry and providing services independently in the GNSS unavailable environment. Many error items of pseudolite positioning system, e.g., tropospheric delay error, need to be corrected by an accurate model. While several tropospheric delay models suitable for pseudolite positioning systems have been proposed, the key parameters indicating the upper boundaries for tropospheric refraction are fixed to an experimental value in these models. In this paper, we studied the spatiotemporal characteristics of the upper boundary heights for hydrostatic and wet tropospheric delay based on the ERA5 global meteorological reanalysis data. With the refined height boundary term, we refine four existing tropospheric delay models for pseudolite positioning systems, including RTCA, MRTCA, Bouska and Hopfield models. To evaluate the performance of the refined models, we selected 12 airports distributed globally as experimental areas and analyzed the error characteristics of the four refined tropospheric models and the LTC model (independent of height). The experimental results show that when the slant distance between the pseudolite base station and the receiver is constant at 5 km, the MRTCA model has the best performance, with an RMSE (root mean square error) of about 0.15 m. When the elevation angle between the pseudolite base station and the receiver is constant, the RMSE of the LTC model is the smallest at the low elevation angle, and the RMSE of the MRTCA model is the smallest at the high elevation. The RMSE of pseudolite tropospheric delay models show seasonal variation.

Keywords: Pseudolite; Troposphere Delay Model; NWM Ray-tracing

1. Introduction

GNSS (Global Navigation Satellite System) is a system that uses satellites orbiting the earth and controls auxiliary equipment on the ground to provide positioning, navigation and timing (PNT) services covering the whole world (Yang, 2016, 2017, 2018). GNSS satellites operate in orbits approximately 20000 km away from the Earth's surface. The navigation signals received by the user receivers on the ground are very weak, and they are vulnerable to various interference from the external environment. For users in complex environments such as indoor, underground, dense forests or urban canyons, the signal strength may be too weak or even completely undetectable, resulting in the failure to use GNSS PNT services.

Various alternative and enhanced auxiliary system are being developed (Reid et al., 2015; Ge et al., 2018; Park et al., 2020; Li et al., 2020; Li et al., 2022), where ground-based pseudolite positioning system has been widely studied and applied (Kim et al., 2014; Sheng et al., 2020; Fan et al., 2022). The ground-based pseudolite positioning system is mainly composed of two parts: base station and user receiver. The base station, also known as

* Corresponding author.
E-mail address: junping@shao.ac.cn (J. Chen).

https://doi.org/10.1016/j.asr.2024.02.034
0273-1177/

pseudolite (PL), is a device used to generate and transmit signals similar to GNSS. The ground-based pseudolite positioning system can not only serve as an auxiliary GNSS enhancement system in the GNSS challenging environment but also establish an independent positioning system in the case of GNSS signal failure (Fan et al., 2021; Tang et al., 2021).

In the field of civil aviation, the most widely used landing system is the ILS (Instrument Landing System). However, due to the inherent defects of ILS navigation signals (signals are easily reflected and refracted by buildings and other objects), it is necessary to have a large interval when using ILS system for landing (Liu et al., 2006). The airport landing system based on pseudolite is flexible and has strong anti-interference ability. Its low-cost characteristics are of great significance for various types of airports, and therefore have received increasing attention. During the process of takeoff and landing, the area crossed is relatively large, so it is necessary to consider the impact of tropospheric delay on the positioning of pseudolite positioning system (Wang, 2002; Wang and Wang, 2007).

Compared with GNSS satellites, pseudolites are very close to the user receiver, usually in the range of several hundred meters to several kilometers. Therefore, there are many differences between the pseudolite positioning system and GNSS in error sources and processing methods (Guo et al., 2018; Sun et al., 2021; Sun and Wang, 2022). Compared with GNSS satellite orbit error, the position of the ground-based pseudolite base station is usually fixed and can be accurately measured (Rizos et al., 2010; Rizos, 2013). In addition, due to the low altitude of the pseudolite working environment, the ionospheric delay error is usually not considered. Tropospheric delay error becomes particularly important in pseudolite positioning system, especially in the application of airports, where aircrafts are operating in a relatively large area during takeoff and landing, and the tropospheric delay error has a large impact on the estimation of height component (Jiang et al., 2015).

The pseudolite signal transmission path is approximately horizontal in the lower troposphere, tropospheric delay estimation is very difficult (Trunzo et al., 2011). The tropospheric delay model used in GNSS cannot be directly used to estimate the tropospheric delay in pseudolite positioning system (Tuka and El-Mowafy, 2013). Based on the tropospheric delay model of GNSS, some tropospheric delay models suitable for pseudolite positioning systems are developed, such as the RTCA (RTCA, 2000), MRTCA (Biberger et al., 2003), Hopfield (Hofmann-Wellenhof et al., 2000), Bouska (Bouska and Raquet, 2003) and LTC (Wang et al., 2005) model. The RTCA and Hopfield model for pseudolite positioning system is developed through an integration method, where the atmospheric refractive index is modeled according to the altitude, and then integrated along the signal propagation path between the pseudolite base station and the user receiver. The LTC model assumes that the tropospheric delay is proportional to the distance between the pseudolite base station and the user receiver, and uses the distance proportion method to estimate the tropospheric delay of the pseudolite positioning system (Barnes et al., 2007).

These tropospheric models for pseudolite positioning systems have been proposed in the past few years, but there are few experiments to evaluate the performance of these models. Furthermore, these experiments which are usually conducted under standard atmospheric conditions at sea level are used to compare the above models (Wang et al., 2005; Choudhury et al., 2009; Ahmed et al., 2013; So et al., 2013; Zhang et al., 2014), which differ significantly from the actual work environment of pseudolite positioning system. In addition, the troposphere models mentioned above (except for the LTC model, which is only related to distance) all use fixed values as cutoff heights for dry and wet delays, ignoring their spatiotemporal characteristics, which will inevitably lead to certain model errors. In this paper, we divide the global region into a grid of $1^\circ \times 1^\circ$ and use ERA5 global meteorological reanalysis data to fit the cutoff heights of dry and wet delays at grid points. The cutoff heights of dry and wet delay can be obtained by bilinear interpolation through fitting parameters of the nearest 4 grid points in the user area. The refined models were compared with the original models using the most accurate NWM (Numerical Weather Model) ray-tracing method for tropospheric delay estimation in the GNSS field. 12 important airports around the world were selected as the experimental areas to analyze the error characteristics of the refined troposphere delay models for pseudolite positioning system.

This paper consists of 4 sections. The second section introduces common tropospheric delay models for pseudolite positioning system, refines the model by fitting the cutoff heights of dry and wet components, and outlines the experimental data and evaluation methods. The third section assesses the refinement in the tropospheric model and analyzes its characteristics. Section 4 summarizes the full research.

2. Data and methods

Existing tropospheric models for pseudolite positioning system often rely on empirically fixed values as cutoff heights for tropospheric dry and wet delays. However, adopting the same global empirical values overlooks the spatiotemporal variations of these cutoff heights. Therefore, there is a need to model the cutoff heights considering factors such as time, longitude, latitude, and others to enhance the precision of the existing model.

To evaluate the effectiveness of the refined models, this study selected 12 significant airports globally as our experimental areas. This paper utilized the results of the NWM ray-tracing single-difference method as reference values for tropospheric delay between pseudolite base stations and the receiver. ERA5 data was employed as input for

meteorological data to minimize the impact of other factors on the results.

2.1. Common troposphere models for pseudolite positioning system

The tropospheric delay consists of a hydrostatic (dry) component and a wet component:

$$\Delta L_{trop} = \Delta L_{dry} + \Delta L_{wet} \tag{1}$$

Radio Technical Commission for Aeronautics (RTCA) has defined a tropospheric delay model for the use of Local Area Augmentation System (LAAS) (RTCA, 2000). Eq. (2) determines the hydrostatic and wet component respectively.

$$\Delta L_{trop} = 10^{-6} \cdot N_{*,0} \cdot D \cdot \left(1 - \frac{h_{rov} - h_{pl}}{h_{*,0}}\right) \tag{2}$$

Where, '*' represents the parameter of the dry or wet component, D is the slant distance between the pseudolite station and the user receiver, h_{rov} is the height of the user receiver, h_{pl} is the height of the pseudolite station, $h_{*,0}$ is a fixed scaled height for the model. From experience, $h_{dry,0}$ and $h_{wet,0}$ are usually set as 42700 m and 12000 m. These heights are arbitrarily defined as the upper boundaries for tropospheric refraction. The refractive index $N_{*,0}$ are obtained from meteorological data, which can be calculated by Eq. (3).

$$\begin{cases} N_{dry} = 77.6 \cdot \frac{P}{T} \\ N_{wet} = 22770 \cdot \frac{f}{T^2} \cdot 10^{\frac{7.4475 \cdot (T-273)}{T-38.3}} \end{cases} \tag{3}$$

Where, P is the atmospheric pressure in mbar, T is the temperature in Kelvin, f is the relative humidity in percentage (%). It is important to note that these parameters have to be reduced at sea level before they can be used in Eq. (2).

It can be seen from Eq. (2) that the RTCA model only focuses on the primary term of the ratio of the height difference between the pseudolite station and the user receiver to the fixed scaled height. Biberger et al. (2003) proposed some modifications to the RTCA model by considering the high-order terms. The modified RTCA (MRTCA) model is shown in Eq. (4):

$$\Delta L_{trop} = 10^{-6} \cdot N_{*,0} \cdot R_{rov} \cdot \left(1 - 2 \cdot \frac{h_{rov} - h_{pl}}{h_{*,0}} + 2 \cdot \frac{h_{rov}^2 + h_{rov} \cdot h_{pl} + h_{pl}^2}{h_{*,0}^2}\right) \tag{4}$$

Where, R_{rov} is the slant distance between the pseudolite station and the user receiver, and other terms have the same meaning as in Eq. (2).

Hofmann-Wellenhof et al. (2000) directly derived the troposphere delay model for pseudolite positioning system from the Hopfield model, which is an integral from the sea level surface.

$$\Delta L_{trop} = 2 \cdot 10^{-7} \cdot N_{*,0} \cdot R_{rov} \cdot \left(\left(1 - \frac{h_{rov}}{h_{*,0}}\right)^5 - \left(1 - \frac{h_{pl}}{h_{*,0}}\right)^5\right) \cdot \frac{h_{*,0}}{h_{rov} - h_{pl}} \tag{5}$$

Bouska and Raquet (2003) derived the pseudolite tropospheric model related to the refractive index N_* at the height of the pseudolite station from the Hopfield model. This is also the difference between Bouska model and the other three models above.

$$\Delta L_{trop} = 2 \cdot 10^{-7} \cdot N_* \cdot R_{rov} \cdot \left(1 - \left(1 - \frac{h_{rov} - h_{pl}}{h_{*,0} - h_{pl}}\right)^5\right) \cdot \frac{h_{*,0} - h_{pl}}{h_{rov} - h_{pl}} \tag{6}$$

Length based tropospheric delay model (LTC) assumes that distance between the pseudolite station and the user receiver have atmospheric effects (refractivity index) proportional to the length of the line. The refractivity index (N) is usually calculated by the constants. Here the LTC model is given by Eqs. (7)–(9):

$$\Delta L_{trop} = 10^{-6} \cdot N \cdot D \tag{7}$$

$$N = 77.689 \cdot \frac{P - e}{T} + 71.2952 \cdot \frac{e}{T} + 375463 \cdot \frac{e}{T^2} \tag{8}$$

$$e = 6.1078 \cdot \exp\left(\frac{17.269 \cdot (T - 273.15)}{237.30 + (T - 273.15)}\right) \cdot f \tag{9}$$

Where, the meanings of D, P, T and f are the same as those of the pseudolite tropospheric delay models introduced above. It can be seen from the Eqs. (7)–(9) that in LTC model, the tropospheric delay is independent of the height difference between the pseudolite station and the user receiver.

2.2. Refinement of troposphere models for pseudolite positioning system

The troposphere models introduced above (except the LTC model) use $h_{*,0}$ obtained from the empirical model. We improved the accuracy of the pseudolite troposphere models by refining the value of $h_{*,0}$.

By definition, we designate the height atmospheric pressure reaches 0 Pa as $h_{dry,0}$, and the height where specific humidity reaches 0 g/kg as $h_{wet,0}$. However, it's important to note that in reality, atmospheric pressure cannot reach exactly 0 Pa, although it can approach very close to this ideal value in certain situations.

ERA5 is the fifth generation of ECMWF (European Centre for Medium-Range Weather Forecasts) atmospheric reanalysis of the global climate covering the period from January 1950 to the present. ERA5 provides hourly estimates of a large number of atmospheric, land and oceanic climate variables (Joaquín et al., 2021). ERA5 includes information about uncertainties for all variables at reduced spatial and temporal resolutions. ERA5 combines vast

amounts of historical observations into global estimates using advanced modeling and data assimilation system. ERA5 comprises 37 layers of atmospheric pressure data, with the highest layer reaching a minimum value of just 1 Pa (Zhu et al., 2022). According to the Saatamoinen model (SAASTAMOINEN, 1972), the maximum impact of an atmospheric pressure of 1 Pa on tropospheric delay does not exceed 2 mm. Therefore, the atmospheric height at 1 Pa can be considered as $h_{dry,0}$. The height at which the specific humidity at the grid point first reaches 0 g/kg can be determined using ERA5 data. By applying polynomial fitting to the layered data in the vicinity of this height, $h_{wet,0}$ can be obtained.

We select the ERA5 global grid data (including geopotential height, temperature, atmospheric pressure, and specific humidity with resolution of 1°×1°) from 2020 to 2022, and analyze the relationship between the scaled height ($h_{dry,0}$ and $h_{wet,0}$), latitude and longitude, and the day of the year (DOY). Atmospheric dry delay accounts for 90 % of the total tropospheric delay, so it is important to correctly estimate the atmospheric dry delay. Fig. 1 shows the relationship between $h_{dry,0}$ and latitude and longitude in different seasons.

From a global perspective (Fig. 1), the value of $h_{dry,0}$ ranges from 40,000 to 50000 m, and most grid points have values larger than 42700 m, which also shows that the direct selection of the fixed value of $h_{dry,0} = 42700$ m will cause a certain error. From the perspective of the whole year, the value of $h_{dry,0}$ does not change much at the same latitude and different longitudes. However, in April and October, at the same longitude, the value of $h_{dry,0}$ gradually decreases from the equator to the north and south, and is roughly symmetrical along the equator. In January, at the same longitude, the value of $h_{dry,0}$ gradually decreases from the south to the north. In July, at the same longitude, the value of $h_{dry,0}$ gradually decreases from the north to the south.

As can be seen from Fig. 1, using fixed empirical value $h_{dry,0}$ globally can lead to errors in the tropospheric delay model. In the annual time series, $h_{dry,0}$ also has a certain trend of change. Therefore, it is possible to fit $h_{dry,0}$ using annual and semiannual terms. By using the above ERA5 data from 2020 to 2022, we determine the mean values (A_0) as well as annual (A_1,A_2) and semiannual amplitudes (A_3,A_4) for selected parameters $h_{dry,0}$ on a regular 1°×1° grid, as follows:

$$h_{dry,0} = A_0 + A_1 \cos\left(\frac{\mathrm{DOY}}{365.25} 2\pi\right) + A_2 \sin\left(\frac{\mathrm{DOY}}{365.25} 2\pi\right) + A_3 \cos\left(\frac{\mathrm{DOY}}{365.25} 4\pi\right) + A_4 \cos\left(\frac{\mathrm{DOY}}{365.25} 4\pi\right) \quad (10)$$

Where, DOY is the day of the year.

The relationships between $h_{wet,0}$, latitude and longitude are not obvious (Fig. 2). From a global perspective, the value of $h_{wet,0}$ ranges from 0 to 12000 m, and most grid points have values less than the experience fixed value. Therefore, it is not proper to directly set $h_{wet,0}$ as 12000 m. The daily variation of wet delay is pronounced, despite constituting only 10 % of the total tropospheric delay. Therefore, we calculated the annual average of $h_{wet,0}$ at each grid point and used this value as the grid product.

2.3. Experimental data and evaluation method

Previous studies usually used the standard atmospheric environment ($P_0 = 1013.25$ mbar, $T_0 = 18$ ℃, $H_0 = 50$ %) at sea level to compare different pseudolite tropospheric delay models. However, in the actual use of the pseudolite positioning system, the location of the pseudolite receiver

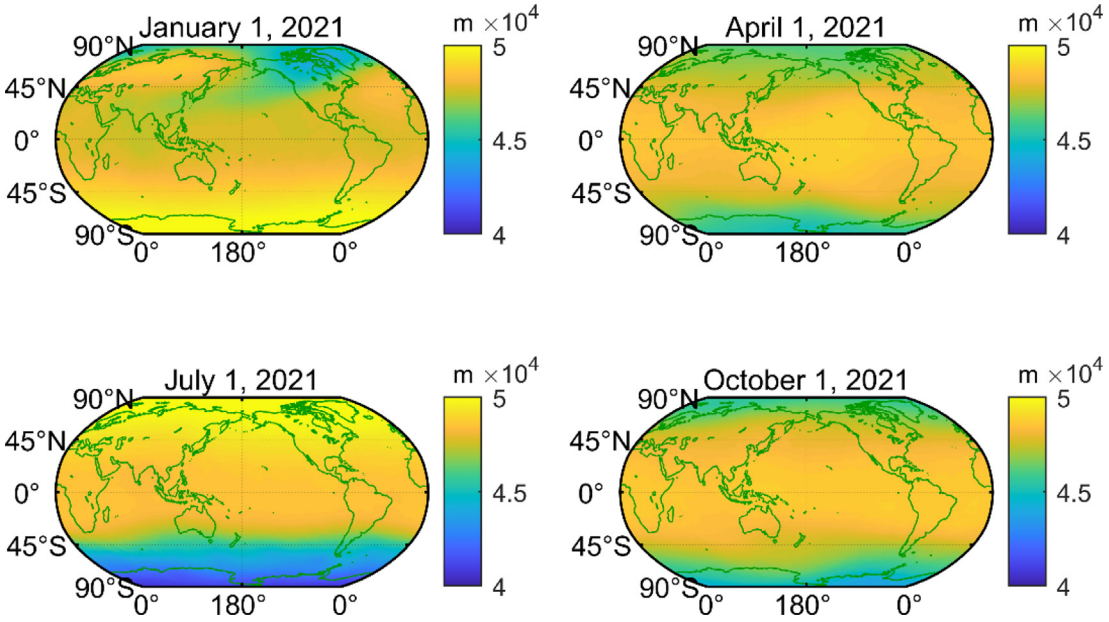

Fig. 1. The relationship between $h_{dry,0}$ and latitude and longitude in different seasons.

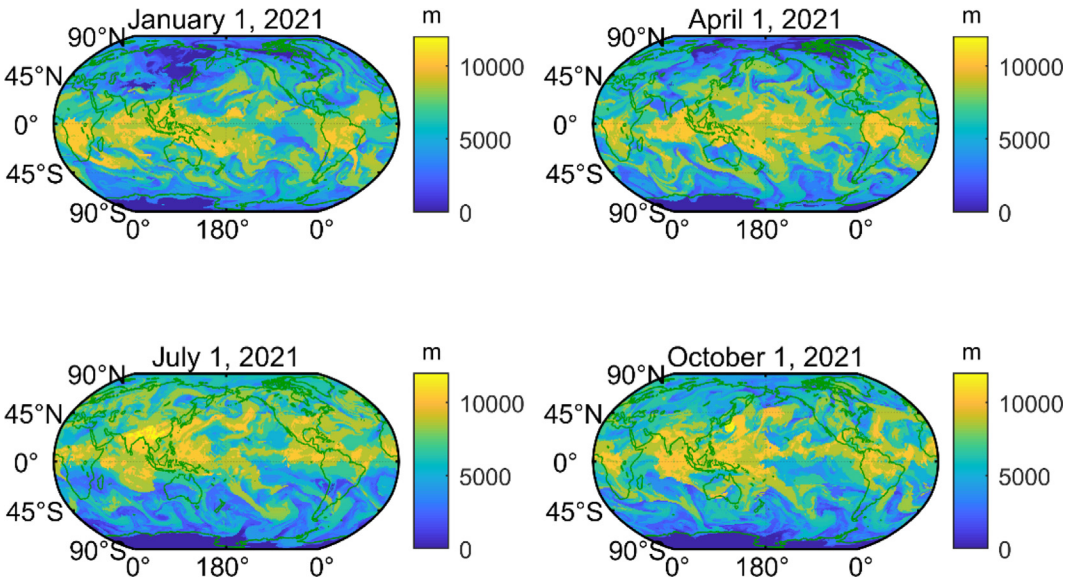

Fig. 2. The relationship between $h_{wet,0}$ and latitude and longitude in different seasons.

and meteorological parameters (atmospheric pressure, temperature, and relative humidity) cannot be in standard conditions. Therefore, it is necessary to evaluate the above pseudolite tropospheric models in real situations.

In this paper, we have selected ERA5 global grid data spanning from 2020 to 2022. Using bilinear interpolation, we have obtained the corresponding meteorological values for the experimental areas. Such experiments using meteorological values derived from real reanalysis data are inherently more reliable than relying on a standard atmospheric environment.

In order to better compare the results of the above pseudolite tropospheric delay models in practical applications, 12 airports around the world were selected as experimental areas (Fig. 3). Their corresponding latitude, longitude and altitude are obtained from the official website.

Previous studies only evaluated the relative error between different tropospheric delay models but did not get the absolute error. The NWM ray-tracing method is a high-precision electromagnetic wave delay correction method based on Snell's law, assuming that the tropospheric atmosphere is spherically stratified (Landskron and Böhm, 2018; Zus et al., 2021). By using ERA5 reanalysis data to obtain the meteorological data in the experimental areas, the reference value of tropospheric delay in the experimental areas can be obtained through the ray-tracing method, and the accuracy of the above pseudolite tropospheric delay models can be evaluated. Since both the pseudolite troposphere models and the ray-tracing method use ERA5 data, the impact of diverse meteorological data on the results can be avoided. Due to the influence of the curvature of the earth, the elevation angles of two points on the same ray on the earth are different. The schematic diagram of NWM ray-tracing method is shown in Fig. 4.

When the altitude of the pseudolite and the receiver together with the elevation angle from the pseudolite to

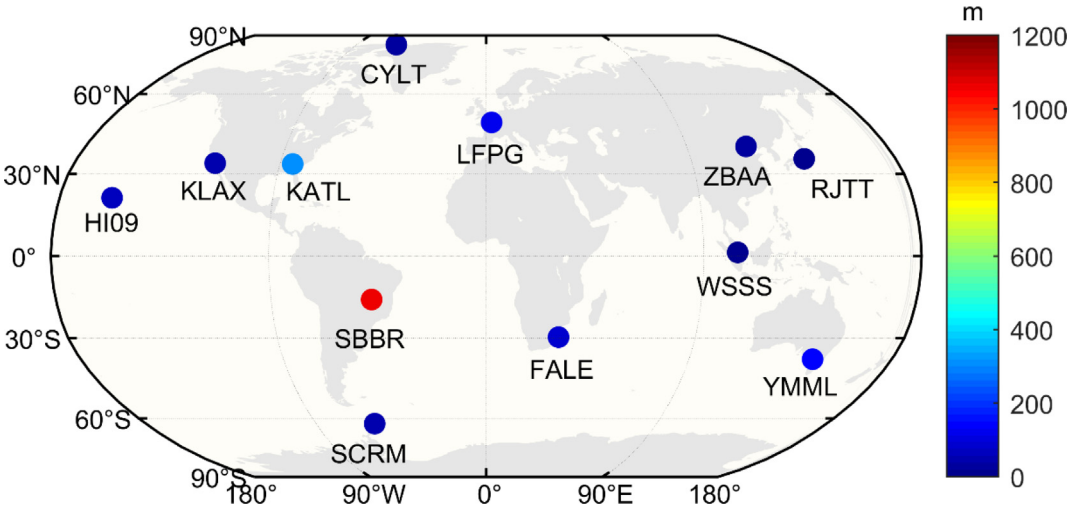

Fig. 3. Global distribution of selected airports.

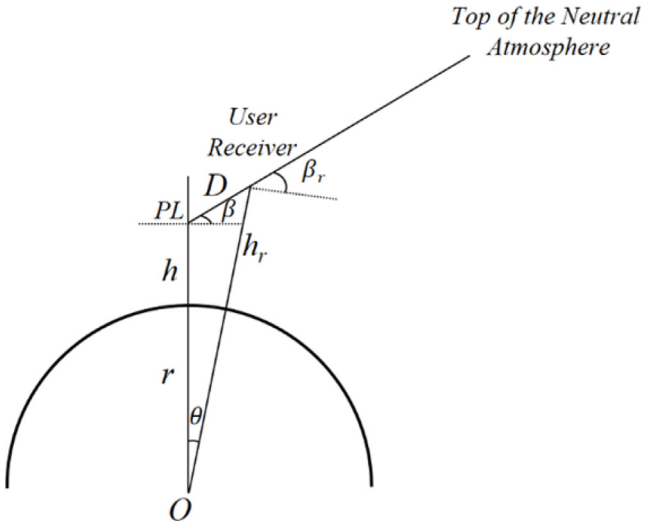

Fig. 4. Schematic diagram of ray-tracing method.

the receiver are known, the elevation angle at the receiver can be calculated by the following equation:

$$h_r = \sqrt{(r+h)^2 + D^2 - 2\times(r+h)\times D\times\cos(\beta+\pi/2)} - r = \sqrt{(r+h)^2 + D^2 + 2\times(r+h)\times D\times\sin\beta} - r \tag{11}$$

And,

$$\beta_r = \beta + \theta = \beta + \arcsin\left(D\cdot\sin(\beta+\pi/2)/(r+h_r)\right) = \beta + \arcsin\left(D\cdot\cos\beta/(r+h_r)\right) \tag{12}$$

Where, D is the slant distance between the pseudolite station and the user receiver, O is the center of the earth, r is the mean radius of the earth, h is the altitude of the pseudolite, h_r is the altitude of the receiver, β is the elevation angle from the pseudolite to the receiver, θ is the angle between the pseudolite and the receiver and the earth center, β_r is the elevation angle at the receiver.

It should be noted that when the elevation angle between the pseudolite and the receiver is very small, even if the elevation angle is corrected, the ray-tracing difference method still has a large error in calculating the pseudolite tropospheric delay. Therefore, the following discussion does not consider the case where the elevation angle is too low (less than 5°).

3. Results and analysis

Firstly, we assessed the fitting performance of the pseudolite troposphere dry and wet delay cutoff heights. Subsequently, the effectiveness of the refined models was evaluated in the experimental regions of 12 airports. Finally, we analyzed the characteristics of the refined pseudolite troposphere models, considering aspects such as elevation angle, slant distance, and seasonality.

3.1. Evaluation of refined troposphere models for pseudolite positioning system

Tropospheric delay is closely related to latitude and has a lower correlation with longitude (Ding et al., 2023). Therefore, we present the fitting results for five stations uniformly distributed in latitude at the same longitude (Fig. 5(a)-(e)). In the figure, the dark blue dots represent the daily $h_{dry,0}$ calculated from the ERA5 data spanning the years 2020 to 2022. The value of $h_{dry,0}$ fitted according to Eq. (10) describes the actual annual variation and semi-annual cycle particularly well over the selected time span (red lines). The purple line represents the fitting residuals between the two. And, the light blue line represents the fixed value $h_{dry,0} = 42700$ used in the original models. It is evident that there is a significant deviation between the actual daily $h_{dry,0}$ and the fixed value. The method proposed in this article effectively fits the time series of $h_{dry,0}$. From a global perspective, the fitting residuals are all less than 0.6 km, and the $h_{dry,0}$ obtained by fitting is not much different from the actual cutoff height of dry delay (Fig. 5(f)).

$h_{dry,0}$ and $h_{wet,0}$ are globally expressed in the form of a grid, and the resolution can be adjusted as needed. After obtaining the five grid coefficients($A_0 \sim A_5$) of $h_{dry,0}$ and the values of $h_{wet,0}$ for the four grid points around a station, the values of $h_{dry,0}$ and $h_{wet,0}$ at the station can be calculated with bilinear interpolation.

To validate the stability of the gridded product provided in this paper, we conducted gridded modeling of tropospheric delay cutoff height using data from the three years 2020–2022 and the single year 2021. Additionally, we selected the first day of each month from January to October 2023 (up to the present) to compare the three-year and one-year gridded products. The experiment was conducted in the previously mentioned 12 airports as the test area, with the elevation angle between the pseudolite base station and the receiver set at 45° and the slant distance set at 5000 m. We calculated the mutual differences by averaging the results of the two gridded products for each station, as shown in Figs. 6 and 7.

Fig. 6 shows that using the two gridded products, the cutoff height for the dry delay (Fig. 6(a)) differs by only about 60 m at most, and for the wet delay (Fig. 6(b)), the variation is more pronounced, but the difference is still less than 90 m. We believe that such small discrepancies are acceptable compared to the dry delay cutoff heights of 40000–50000 m and wet delay cutoff heights of around 12000 m.

Fig. 7 indicates that using the two gridded products, the maximum difference in tropospheric delay is less than 0.3 mm. Therefore, we believe that the duration of the fitted data has a minimal impact on the results in this study. For the subsequent analyses, we will utilize the gridded products from the three-year dataset.

We selected ERA5 data from January 1, 2023, to validate the effectiveness of the proposed method. At present,

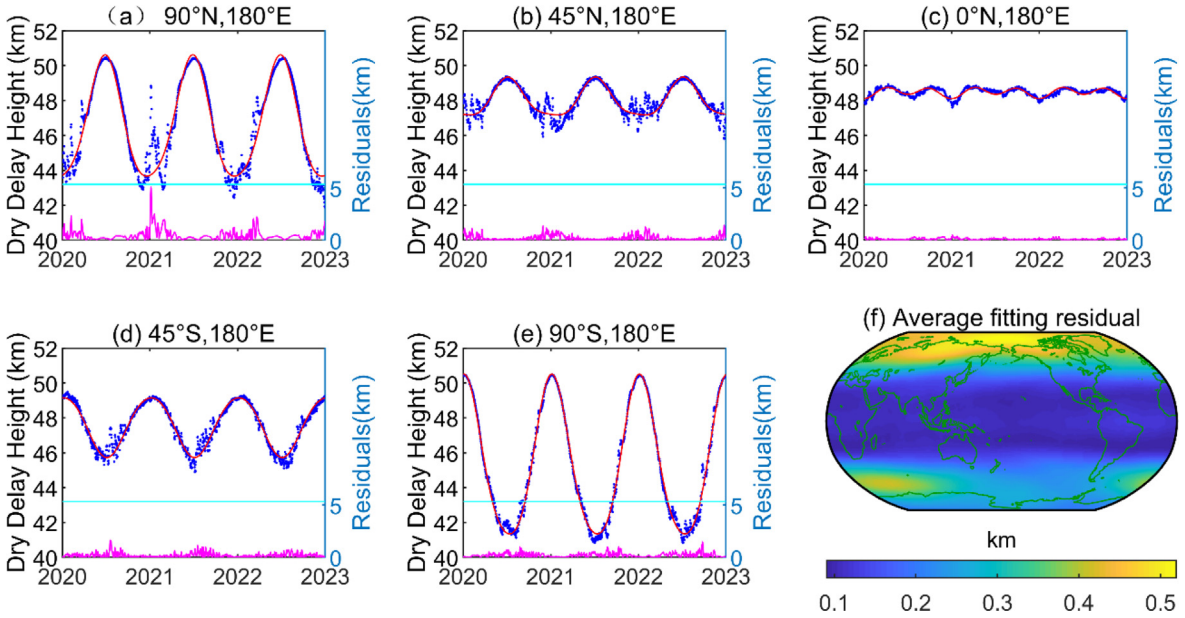

Fig. 5. Fitting diagram of dry delay height. (a)–(e) The fitting situation of grid points on 180°E and different longitudes. (f) Annual average fitting residuals.

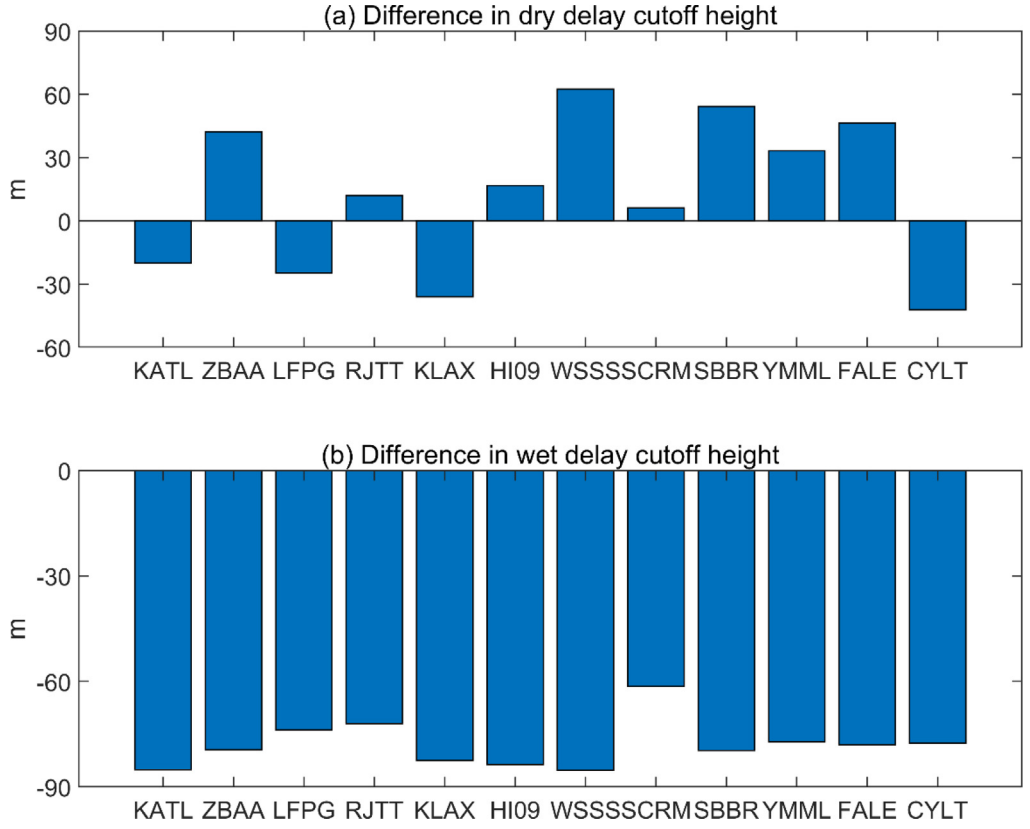

Fig. 6. Comparison of tropospheric fitting cutoff heights between three-year and one-year gridded products.

the signal service range of a single pseudolite base station is approximately 5000 m. Therefore, in the experimental area of the 12 airports, we selected the slant distance of 5000 m between the pseudolite base station and the receiver. The elevation angle varied from 5° to 90° with a 1° interval. In each elevation angle, the tropospheric delay was calculated using the method proposed in this paper and the original models. The RMSE of the results at all elevation angles was taken as the tropospheric delay error for each station.

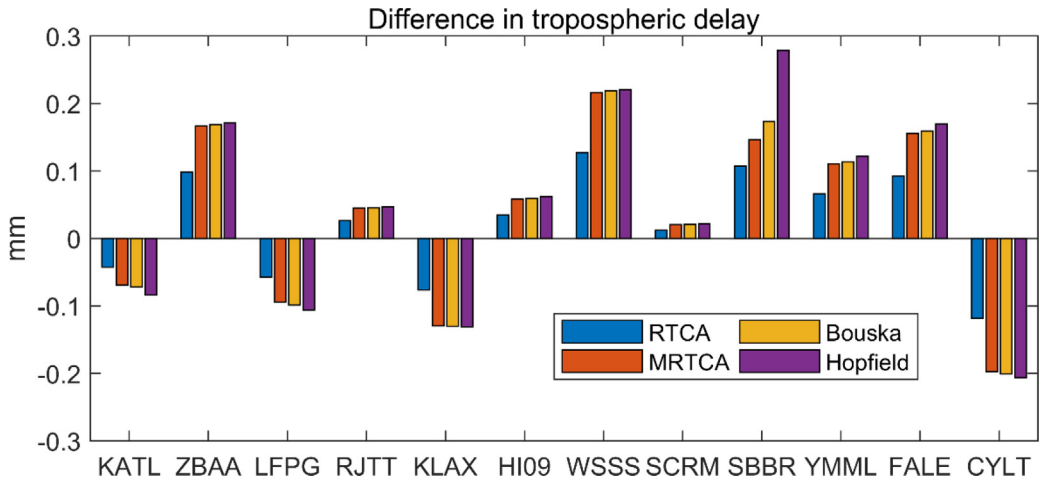

Fig. 7. Comparison of tropospheric delay modeled using three-year and one-year gridded products.

The values of $h_{dry,0}$ and $h_{wet,0}$ calculated by the grid and the fixed values are substituted into the above tropospheric delay models for comparison, and the results are shown in Fig. 8. The results of the RMSE (root mean square error) for different tropospheric delay models at each station when the slant distance is 5000 m. It can be found that the correction of $h_{*,0}$ reduces the delay error of different tropospheric models to a certain extent. The accuracy of pseudolite troposphere models can be refined by using grid interpolation to correct $h_{*,0}$, where the improvement reaches 2.5, 3.2, 3.1 and 3.6 cm for the RTCA, MRTCA, Bouska, and Hopfield model respectively. Compared to the original models, the new models have improved by 17.1 %, 25.6 %, 23.3 % and 26.1 %, respectively.

3.2. Characteristics of refined tropospheric delay models for pseudolite positioning system

3.2.1. Elevation angle related pattern

According to the principle of refraction, the degree of refraction effect depends on the density of the medium and the angle of incidence. Therefore, the elevation angle of the line of sight affects the propagation path and delay of the signal in the atmosphere, which in turn affects the magnitude of the tropospheric delay error. Therefore, the pseudolite tropospheric delay is related to the elevation angle between the pseudolite station and the receiver.

Fig. 9 illustrates the pseudolite tropospheric delays calculated from the five refined models and NWM ray-tracing method at a slant distance of 5000 m, with the ele-

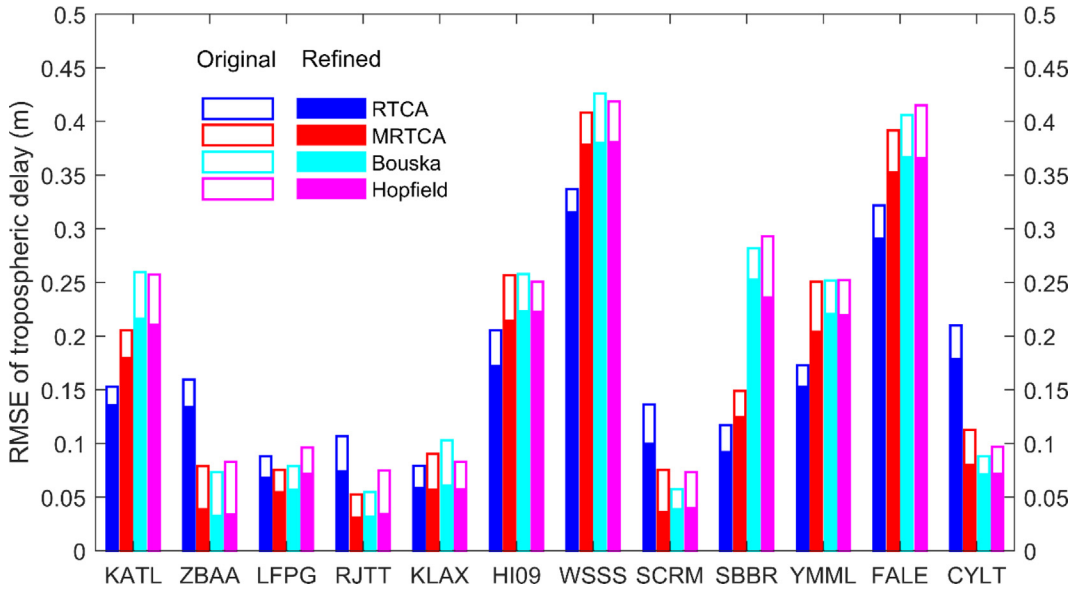

Fig. 8. RMSE of different tropospheric delay models before and after improvement. (The slant distance is 5000 m, the elevation angle varies from 5° to 90°, and the interval is 1°. The hollow bar chart represents the fixed value of $h_{*,0}$ directly used in the original tropospheric delay models, the solid bar chart represents the new value of $h_{*,0}$ obtained after grid interpolation in the refined tropospheric delay models, and the different part indicates the improvement.).

vation angle varying from 5° to approximately 90°. When the elevation angle is less than 5°, the ray-tracing method cannot fully correct for the effect of the earth curvature, so the results with the elevation angle less than 5° are not compared.

Taking the RJTT station (Fig. 9(a)) and the KLAX station (Fig. 9(b)) as examples, it can be observed that the LTC model only takes into account the slant distance and does not consider the elevation angle. When the slant distance is 5000 m, the results of the LTC model are fixed values, which are significantly larger than the true pseudolite tropospheric delay. Compared with the accurate results obtained by the ray-tracing method ('Radiate' in the Figure), the error of the LTC model gradually enlarges with the increase of the elevation angle, while the errors of the other four models exhibit patterns with elevation angle.

Fig. 9 (c) shows the RMSE of the five refined tropospheric models at different stations using the pseudolite tropospheric delay obtained by the ray-tracing method as the reference true value. The RMSE of pseudolite tropospheric delay is the statistical result at elevation angles range from 5° to 90°. At most stations, the LTC model performs significantly worse compared to the other models, except for the station WSSS, FALE and SBBR. From Fig. 3, it can be seen that these three stations are all located near the equator or in low latitude areas of the southern hemisphere. According to the mean result of the RMSE of the tropospheric delay at all stations, the LTC model has the worst performance of more than 0.4 m. The other four models have little difference of around 0.15 m, and the MRTCA model is slightly better.

3.2.2. Slant distance related pattern

Unlike the GNSS system, the tropospheric delay between pseudolite station and receiver changes with the slant distance between them, even at the same elevation angle. Figs. 10 and 11 show the relationship between the pseudolite tropospheric delay and the slant distance when the elevation angle is constant.

When the elevation angle is 5° and the slant distance is from 0 to 5000 m (10 m as the interval), the results of the above tropospheric delay models and ray-tracing method at different stations are calculated respectively. From the Fig. 10(a) and 10(b), we can find that the pseudolite tropospheric delay is approximately linear with the slant distance when the elevation angle is 5°. Compared with the results of the ray-tracing method, the LTC model has overestimation at different slant distances, and the RTCA, MRTCA, Bouska and Hopfield models all have a certain degree of underestimation.

Fig. 10(c) shows the RMSE of the different tropospheric delay models at different stations, using the results obtained

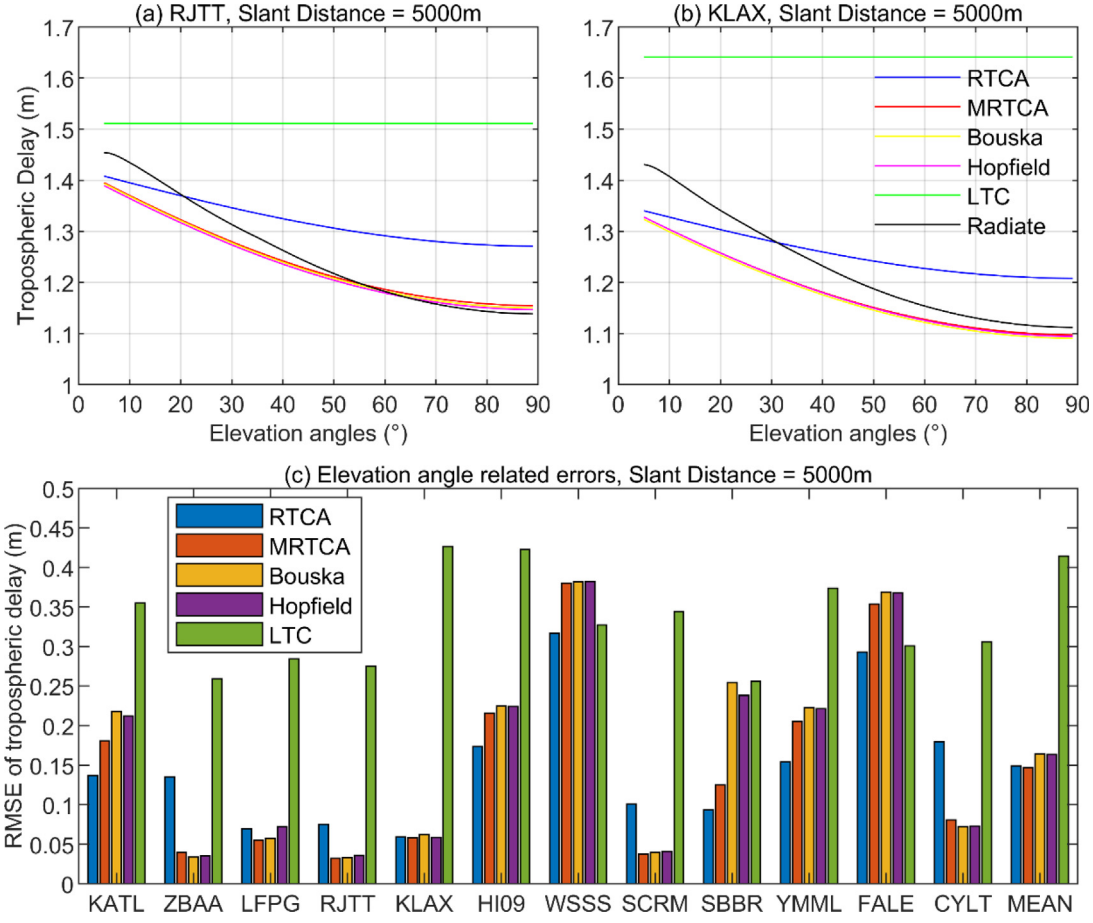

Fig. 9. The characteristics of refined pseudolite tropospheric delay changing with elevation angle.

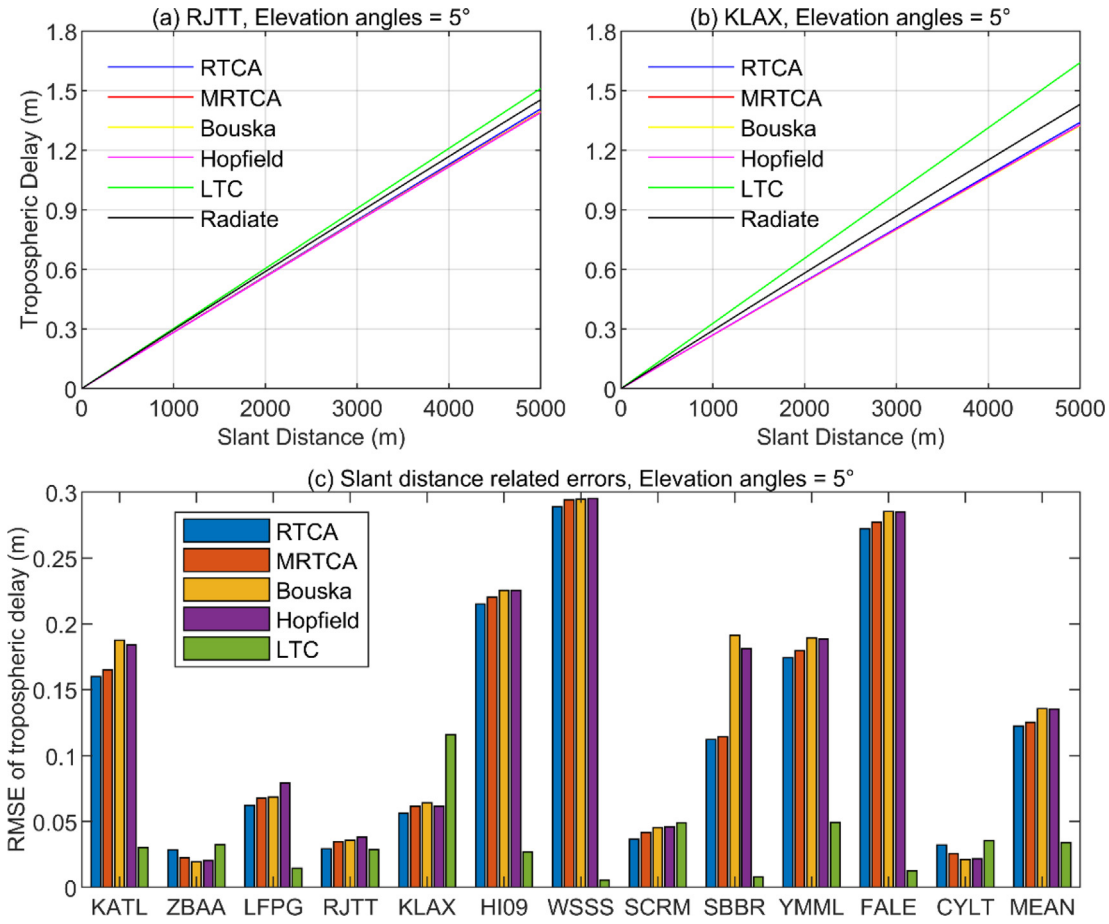

Fig. 10. The characteristics of refined pseudolite tropospheric delay changing with slant distance (Elevation angle = 5°).

by the ray-tracing method as the reference truth value. It can be seen that the existing pseudolite tropospheric delay models have large differences in RMSE at different stations. Stations with small pseudolite tropospheric delay errors can reach about 0.05 m using different models, while stations with large pseudolite tropospheric errors have errors exceeding 0.5 m. Comparing the mean RMSE of different pseudolite tropospheric models at all stations, when the elevation angle is relatively low, the LTC model has the smallest error, with only about 0.04 m. The errors of the other four pseudolite tropospheric models are not much different, all around 0.13 m. Among them, RTCA and MRTCA models are better, and Bouska and Hopfield models are worse.

Fig. 11(a) and 11(b) show the relationship between the pseudolite tropospheric delay and the slant distance when the elevation angle is 80°. According to the pseudolite tropospheric delay calculated by the ray-tracing method, it can be found that when the elevation angle is relatively high, the pseudolite tropospheric delay no longer increases linearly with the increase of the slant distance. However, the current pseudolite tropospheric delay models all assume that the tropospheric delay is linearly related to the slant distance, which will lead to a certain degree of error.

Similarly, the RMSE of different pseudolite tropospheric delay models are also obtained according to the results of ray-tracing method when the elevation angle is 80° (Fig. 11(c)). Comparing the RMSE of different pseudolite tropospheric delay models at all stations, the LTC model has the largest RMSE reaching about 0.2 m, which contradicts the case in lower elevation (e.g., 5°). Compared with the performance at low elevation angle, the other four pseudolite tropospheric delay models perform better at high elevation angles. The RMSE of them are all around 0.1 m, of which the RTCA and MRTCA model have higher accuracy.

3.2.3. Seasonal pattern

The RMSE of pseudolite tropospheric delay not only varies with elevation angle and slant distance but also exhibits seasonal fluctuations. Taking examples from the RJTT station in the northern hemisphere and the FALE station in the southern hemisphere, Fig. 12 illustrates the relationship between the RMSE of pseudolite tropospheric delay and the seasons. It becomes evident that in the northern hemisphere, the RMSE of pseudolite tropospheric delay is smallest around January and reaches its peak around August, while the reverse trend is observed in the southern hemisphere. In general, global tropospheric delay errors are more pronounced in summer and less prominent in winter.

When calculating the tropospheric delay of pseudolites at the same station across different months, we found that

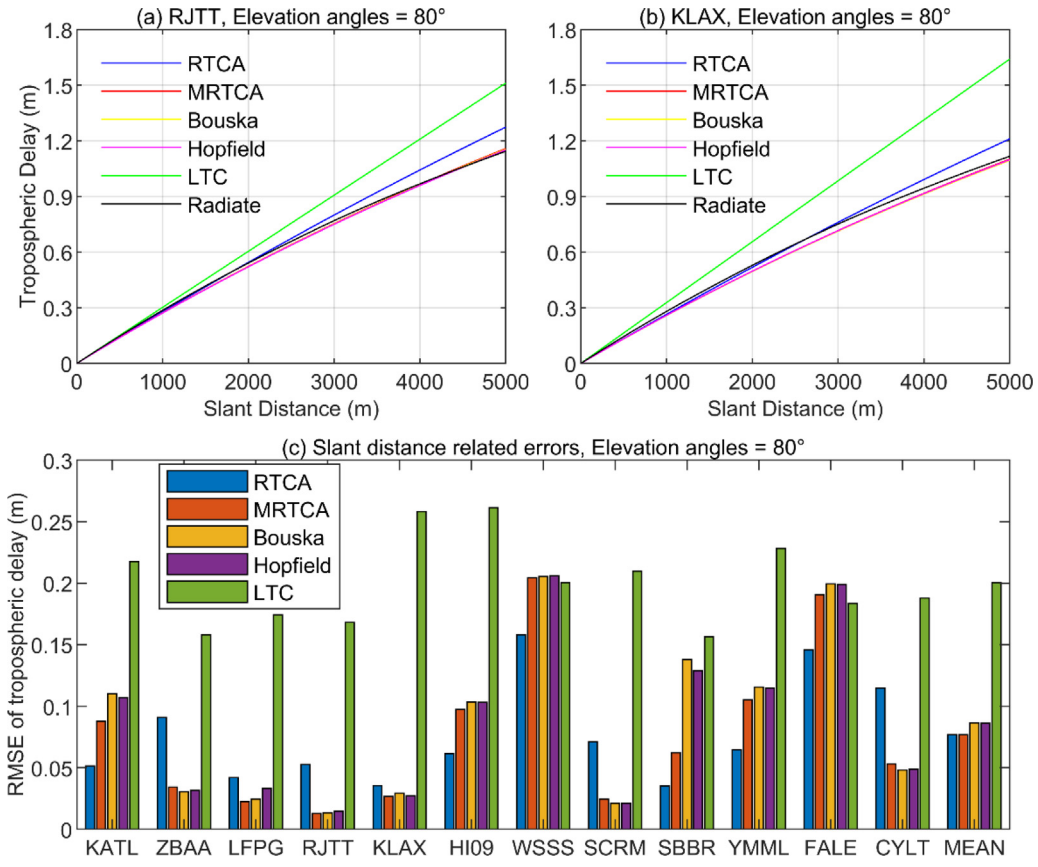

Fig. 11. The characteristics of refined pseudolite tropospheric delay changing with slant distance (Elevation angle = 80°).

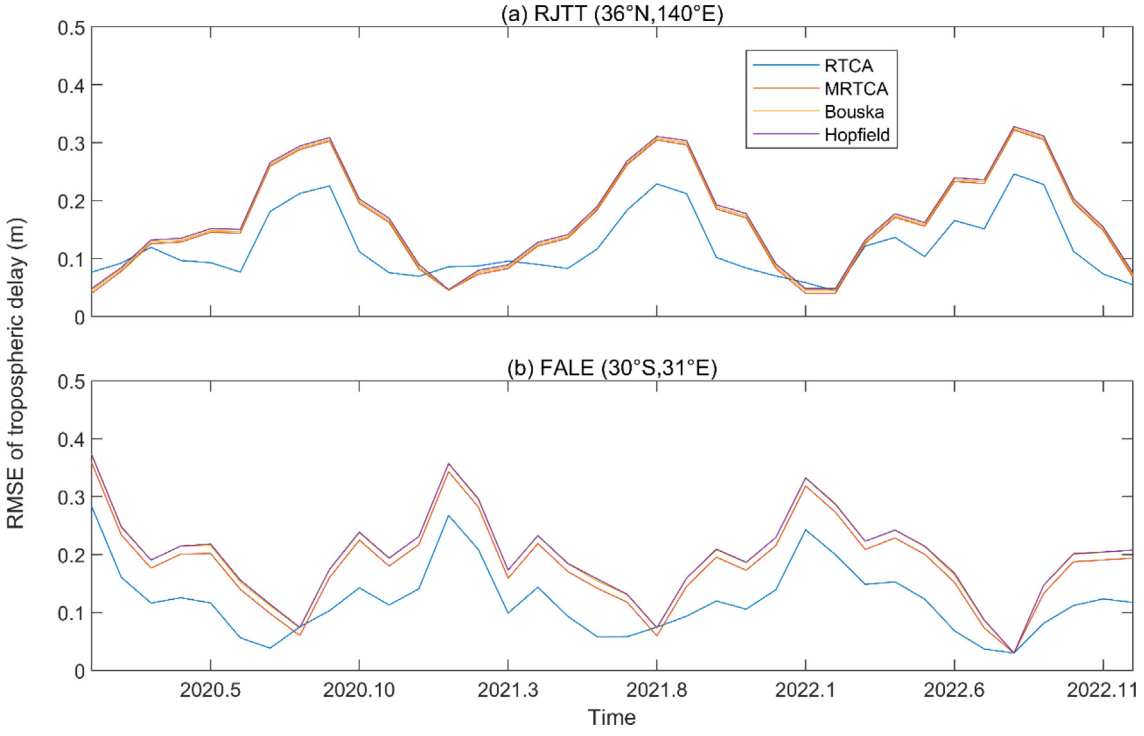

Fig. 12. RMSEs of refined pseudolite tropospheric delay in different months.

the tropospheric delay, calculated according to the model, remains relatively consistent between different months, with differences remaining within 0.1 m. However, the pseudolite tropospheric delay computed using the ray-tracing method is at its highest in summer and lowest in winter, with variations between different months reaching approximately 0.3 to 0.4 m. Consequently, the RMSE of pseudolite tropospheric delay model demonstrates clear seasonal variation. The seasonality in the pseudolite tropospheric model primarily stems from meteorological parameters such as atmospheric pressure, temperature, and relative humidity (Du et al., 2020; Ding et al., 2022; Klos et al., 2023). Nevertheless, owing to factors like the accuracy of meteorological parameters and other variables, the model still exhibits periodic residuals.

4. Discussion and conclusion

Tropospheric delay error is one of the important error sources in the pseudolite positioning system. Unlike the GNSS system, pseudolites cannot eliminate the effects of tropospheric delays through differential positioning techniques, so the accuracy of pseudolite tropospheric models is critical for pseudolite positioning.

In recent years, several tropospheric models appropriate for the pseudolite positioning system have been suggested. However, these models have a limitation in which the key parameters representing the upper boundaries for tropospheric refraction are set to fixed experimental values. In addition, past research of tropospheric delay models for pseudolite positioning systems were simulated under standard atmospheric conditions at sea level, which differs significantly from the actual application scenarios of pseudolite positioning systems.

This paper focuses on investigating the spatiotemporal characteristics of the upper boundary heights for hydrostatic and wet tropospheric delay. To achieve this, we utilize ERA5 global meteorological reanalysis data as the basis for our study. Using a refined height boundary term, we improve four existing tropospheric delay models for the pseudolite positioning system. Taking the tropospheric delay calculated by the ray-tracing method with the highest accuracy as the reference value, we evaluated the performance of the refined four pseudolite tropospheric delay models and the LTC model (independent of height) from different aspects. The following conclusions were reached:

(1) Using a fixed model scaling height ($h_{*,0}$) at any location in the world will introduce errors in the pseudolite troposphere delay model. At the global 1°×1° grid, the critical height of tropospheric hydrostatic delay ($h_{dry,0}$) is modeled with respect to longitude, latitude and the DOY, and the critical height of tropospheric wet delay ($h_{wet,0}$) is meant throughout the year. The stations in the experimental area were interpolated using the grid model to obtain a new $h_{*,0}$. Compared to using the fixed $h_{*,0}$, the RMSE of different tropospheric delay models (RTCA, MRTCA, Bouska and Hopfield models) refined on mean by about 2.5, 3.2, 3.1 and 3.6 cm, respectively. Compared to the original models, the new models have improved by 17.1 %, 25.6 %, 23.3 % and 26.1 %, respectively.

(2) When the slant distance of the pseudolite base station and the receiver is constant at 5000 m, the relationship between the RMSE of different pseudolite tropospheric delay models and the elevation angle are compared. At different stations, the LTC model is significantly worse because it is independent of elevation angle. The results of the other four pseudolite tropospheric models varied across stations. According to the mean results at each station, the LTC model has the worst performance, exceeding 0.4 m, the other four models have little difference, all around 0.15 m, and the MRTCA model is slightly better.

(3) The RMSE of pseudolite tropospheric delay is calculated according to the slant distance between the pseudolite station and receiver, when the elevation angle is constant. The RMSE of different pseudolite tropospheric models vary widely from station to station. At low elevation angles, the pseudolite tropospheric delay is approximately linear with slant distance and increases with slant distance. The RMSE of the LTC model is the smallest, only about 0.04 m. The RMSE of the other four pseudolites tropospheric models are not much different, all around 0.13 m. Among them, RTCA and MRTCA models are better, and Bouska and Hopfield models are worse. At high elevation angles, the pseudolite tropospheric delay no longer increases linearly with slant distance. At different stations, different pseudolite tropospheric delay models have their own advantages and disadvantages. The LTC model has the largest RMSE, which can reach nearly 0.2 m. Compared with low elevation angles, the other four pseudolite tropospheric delay models perform better at high elevation angles, and the RMSE are reduced to a certain extent, about 0.08 m, among which the MRTCA model has the highest accuracy.

(4) The RMSE of pseudolite tropospheric delay is at its minimum in January and peaks in August when stations are located in the northern hemisphere. Conversely, in the southern hemisphere, the pattern is reversed. Generally, global tropospheric delay exhibits a larger RMSE in summer and a smaller one in winter. The pseudolite tropospheric delay calculated according to the models varies only slightly between different months, remaining within 0.1 m. However, the pseudolite tropospheric delay computed using the ray-tracing method is at its highest in summer and at its lowest in winter, with variations between months reaching approximately 0.3 to 0.4 m. Conse-

quently, the RMSE of the pseudolite tropospheric delay model displays seasonal variation. In future studies, a periodic term can be incorporated into the original pseudolite tropospheric delay models to correct for the seasonal variation of pseudolite tropospheric delay errors.

From above, we highly recommend using the MRCTA model due to its superior performance across diverse simulation scenarios. This paper introduces the refined pseudolite tropospheric models based on the ERA5 dataset, with NWM ray-tracing results serving as reference values. Although this approach is optimal under the current conditions, the accuracy of the ERA5 dataset and NWM ray-tracing method may still influence the results. The observational data in existing pseudolite positioning systems have relatively short distances, resulting in minimal tropospheric delay values. This limitation hinders the ability to validate the impact of various refined models on positioning accuracy. In future research, we plan to assess the refined pseudolite tropospheric models from the perspective of positioning results to gain a more comprehensive understanding of their effects.

Declaration of Competing Interest

The authors declare that they have no known competing financial interests or personal relationships that could have appeared to influence the work reported in this paper.

Acknowledgments

This research is supported by the Program of Shanghai Academic Research Leader; the National Key R&D Program of China (No. 2018YFB0504300); Key R&D Program of Guangdong Province (No. 2018B030325001); the National Natural Science Foundation of China (No. 11673050); and the Key Program of Special Development funds of Zhangjiang National Innovation Demonstration Zone (No. ZJ2018-ZD-009). The ERA5 data set used in this study is publicly available at https://cds.climate.copernicus.eu/cdsapp#!/dataset/reanalysis-era5-pressure-levels?tab=form.

References

Ahmed, M.M., Sultana, Q., Reddy, A.S., Malik, M.A., 2013. Tropospheric error correction in assisted GPS signals. Indian J. Radio Space Phys. 42, 159–166.

Barnes, J., Rizos, C., Pahwa, A., et al., 2007. The Potential of locata technology for structural monitoring applications. J. Glob. Position. Syst. 6 (2), 166–172.

Biberger, R.J., Teuber, A., Pany, T., Hein, G.W., 2003. Development of an APL error model for precision approaches and validation by flight experiments. ION, GPS/GNSS, Portland, OR, pp. 2308-2317.

Bouska, C.T.J., Raquet, J.F., 2003. Tropospheric model error reduction in pseudolite based positioning system. ION GPS/GNSS 2003, Portland OR, USA, pp. 390–398.

Choudhury, M., Harvey, B., Rizos, C., 2009. Tropospheric correction for locata when known point ambiguity resolution technique is used in static survey-is it required? IGNSS Symposium 2009. Gold Coast, Australia.

Ding, J., Chen, J., Tang, W., Song, Z., 2022. Spatial-temporal variability of global GNSS-derived precipitable water vapor (1994–2020) and climate Implications. Remote Sens. (Basel) 14, 3493.

Ding, J., Chen, J., Wang, J., et al., 2023. Characteristic differences in tropospheric delay between Nevada Geodetic Laboratory products and NWM ray-tracing. GPS Solutions 27 (1), 47.

Du, Z., Zhao, Q., Yao, W., et al., 2020. Improved GPT2w (IGPT2w) model for site specific zenith tropospheric delay estimation in China. J. Atmos. Sol. Terr. Phys. 2020 (198). https://doi.org/10.1016/j.jastp.2020.105202 105202.

Fan, C., Yao, Z., Yun, S., et al., 2021. Ground-based PPP-RTK for pseudolite system. J. Geod. 95 (12), 133. https://doi.org/10.1007/s00190-021-01589-3.

Fan, C., Yao, Z., Wang, S., et al., 2022. Pseudolite system-augmented GNSS real-time kinematic PPP. J. Geod. 96 (10), 77. https://doi.org/10.1007/s00190-022-01663-4.

Ge, H., Li, B., Ge, M., et al., 2018. Initial assessment of precise point positioning with LEO Enhanced Global Navigation Satellite System (LeGNSS). Remote Sens. (Basel) 10 (7), 984–999. https://doi.org/10.3390/rs10070984.

Guo, X., Zhou, Y., Wang, J., Liu, K., Liu, C., 2018. Precise point positioning for ground-based navigation systems without accurate time synchronization. GPS Solutions 22 (2). https://doi.org/10.1007/s10291-018-0697-y.

Hofmann-Wellenhof, B., Lichtenegger, H., Collins, J., 2000. GPS Theory and Practice, Fifth revised edition. Springer-Verlag Wien, New York, p. 382.

Jiang, W., Li, Y., Rizos, C., 2015. Locata-based precise point positioning for kinematic maritime applications. GPS Solutions 19 (1), 117–128.

Joaquín, M., Dutra, E., Anna, A., et al., 2021. ERA5-Land: a state-of-the-art global reanalysis dataset for land applications. Copernicus GmbH 9. https://doi.org/10.5194/ESSD-13-4349-2021.

Kim, C., So, H., Lee, T., Kee, C., 2014. A Pseudolite-based positioning system for legacy GNSS receivers. Sensors 14, 6104–6123.

Klos, A., Bogusz, J., Pacione, R., et al.,2023. Investigating temporal and spatial patterns in the stochastic component of ZTD time series over Europe. GPS Solutions, 2023.

Landskron, D., Böhm, J., 2018. VMF3/GPT3: Refined Discrete and Empirical Troposphere Mapping Functions. J Geod 92 (4), 349–360. https://doi.org/10.1007/s00190-017-1066-2.

Li, M., Xu, T., Guan, M., et al., 2022. LEO-constellation-augmented multi-GNSS real-time PPP for rapid re-convergence in harsh environments. GPS Solutions 26 (1), 29.

Li, R., Zheng, S., Wang, E., et al., 2020. Advances in BeiDou Navigation Satellite System (BDS) and satellite navigation augmentation technologies. Satellite Navigation 1 (1), 12.

Liu, Y., Chang, W., Chen X., Duan, Y., et al., 2006. The modeling of instrument landing system flight inspection based on global positioning system. Journal of Air Force Engineering University, 2006, 7(4):20-22. https://doi.org/10.1007/s11434-006-2076-2.

Park, K.W., Park, J.I., Park, C., 2020. Efficient methods of utilizing multi-SBAS corrections in multi-GNSS positioning. Sensors 20 (1), 256. https://doi.org/10.3390/s20010256.

Reid, T., Walter, T., Enge, P.K., et al., 2015. Orbital representations for the next generation of satellite-based augmentation system. GPS Solutions 20 (4), 737–750. https://doi.org/10.1007/s10291-015-0485-x.

Rizos, C., Roberts, G., Barnes, J., et al., 2010. Experimental results of locata: A high accuracy indoor positioning system. International conference on indoor positioning and indoor navigation, Zürich, Switzerland, pp. 612–619.

Rizos, C., 2013. Locata: a positioning system for indoor and outdoor applications where GNSS does not work. In: Proceedings of the 18th

Association of Public Authority Surveyors Conference, Canberra, ACT, Australia, pp. 42–47.
RTCA, 2000. GNSS Based Precision Approach Local Area Augmentation System (LAAS)-Signal-in-Space Interface Control Document (ICD). RTCA/DO-246A, Radio Technical Commission for Aeronautics.
SAASTAMOINEN, J., 1972. Contributions to the theory of atmospheric refraction. Bulletin Géodésique (1946-1975), 105(1): pp. 279–298.
Sheng, C., Gan, X., Yu, B., Zhang, J., 2020. Precise point positioning algorithm for pseudolite combined with GNSS in a constrained observation environment. Sensors 20 (4), 1120. https://doi.org/10.3390/s20041120.
So, H., Park, J., Song, K., 2013. Performance analysis of pseudolite tropospheric delay models using radiosonde meteorological data. J. Korean GNSS Society. 2 (1), 49–57. https://doi.org/10.11003/JKGS.2013.2.1.049.
Sun, Y., Wang, J., 2022. Mitigation of multipath and NLOS with stochastic modeling for ground-based indoor positioning. GPS Solutions 26, 47. https://doi.org/10.1007/s10291-022-01230-6.
Sun, Y., Wang, J., Chen, J., 2021. Indoor precise point positioning with pseudolites using estimated time biases iPPP and iPPP-RTK. GPS Solutions 25 (2). https://doi.org/10.1007/s10291-020-01064-0.
Tang, W., Chen, J., Yu, C., et al., 2021. A New Ground-based pseudolite system deployment algorithm based on MOPSO. Sensors 21, 5364. https://doi.org/10.3390/s21165364.
Trunzo, A., Benshoof, P., Amt, J., 2011. The UHARS Non-GPS based positioning system. ION GNSS 2011, Portland, OR, pp. 113–121.
Tuka, A., El-Mowafy, A., 2013. Performance evaluation of different troposphere delay models and mapping functions. Measurement 46 (2), 928–937. https://doi.org/10.1016/j.measurement.2012.10.01.
Wang, J., 2002. Applications of pseudolites in positioning and navigation: progress and problems. J. Glob. Position. Syst. 1 (1), 48–56.
Wang, J.J., Wang, J., 2007. Adaptive tropospheric delay modelling in GPS/INS/Pseudolite integration for airborne surveying. J. GPS 6 (2), 142–148.
Wang, J.J., Wang, J., Sinclair, D., et al., 2005. Tropospheric delay estimation for pseudolite positioning. J. Glob. Position. Syst. 4 (1&2), 106–112.
Yang, Y., 2016. Concepts of comprehensive PNT and related key technologies. Acta Geodaetica Et Cartographica Sinica 45 (5), 505–510. https://doi.org/10.11947/j.AGCS.2016.20160127.
Yang, Y., 2018. Resillient PNT concept frame. Acta Geodaetica Et Cartographica Sinica 47 (7), 893–898. https://doi.org/10.11947/j.AGCS.2018.20180149.
Yang, Y., Yang, C., Ren, X., 2017. PNT Intelligent Services. Acta Geodaetica Et Cartographica Sinica 50 (8), 1006–1012. https://doi.org/10.11947/J.agcs.2021.20210051.
Zhang, R., Huang, X., Li, X.D., 2014. A tropospheric delay estimation method for pseudolite positioning. Journal of Telemetry, Tracking and Command, 35(2), 14-18+59.
Zhu, G., Huang, L., Yang, Y., et al., 2022. Refining the ERA5-based global model for vertical adjustment of zenith tropospheric delay. Satellite Navigation, 2022, 3(3):11.
Zus, F., Balidakis, K., Dick, G., Wilgan, K., Wickert, J., 2021. Impact of tropospheric mismodelling in GNSS precise point positioning: a simulation study utilizing ray-traced tropospheric delays from a high-resolution NWM. Remote Sensing 13 (19), 3944.